PHYSICAL REVIEW B **74**, 035312 (2006)

Electronic and optical properties of InAs/InP quantum dots on InP(100) and InP(311)*B* substrates: Theory and experiment

C. Cornet,[1,*] A. Schliwa,[2] J. Even,[1] F. Doré,[1] C. Celebi,[3] A. Létoublon,[1] E. Macé,[1] C. Paranthoën,[1] A. Simon,[1,3]
P. M. Koenraad,[3] N. Bertru,[1] D. Bimberg,[2] and S. Loualiche[1]
[1]*LENS-UMR FOTON 6082 au CNRS, INSA de Rennes, 20 Avenue des Buttes de Coësmes, CS 14315, 35043 Rennes Cedex, France*
[2]*Institut für Festkörperphysik, Technische Universität Berlin, Hardenbergstrasse 36, 10623 Berlin, Germany*
[3]*COBRA Inter-University Research Institute, Eindhoven University of Technology, P.O. Box 513, NL-5600MB Eindhoven, The Netherlands*

(Received 7 February 2006; revised manuscript received 31 May 2006; published 12 July 2006)

We study the electronic and optical properties of InAs/InP quantum dots (QDs) on (100) and (311)*B* substrates. Atomic force microscopy (AFM) and cross-sectional scanning tunneling microscopy (X-STM) are used to define the size and shape of the quantum dots for calculations. Eight-band $\mathbf{k}\cdot\mathbf{p}$ calculations including strain and piezoelectric effects are then performed on such a structure for two different kinds of substrate orientation (311)*B* and (100). Results for several QD heights found on (311)*B* substrate fit well the experimental data obtained from photoluminescence measurements. On (311)*B* substrate, the shear and hydrostatic deformations are found to be enhanced compared to those on (100) substrate thus affecting the electronic and optical properties. The (311)*B* QDs are found to activate second-order (*S*-*P* channels) transitions resulting from the complete loss of symmetry due to the presence of the piezoelectric field.

DOI: 10.1103/PhysRevB.74.035312 PACS number(s): 73.21.La, 73.22.Dj, 68.37.−d, 71.15.Qe

I. INTRODUCTION

Recently there have been considerable research developments in the field of nanostructured semiconductor materials. In particular, quantum dots (QDs) may improve the properties of high-performance optoelectronic devices as compared to that achieved with semiconductor quantum wells.[1–4] One of the biggest challenges for QD laser devices, however, is to reach the 1.55 μm (0.8 eV) wavelength used for long-haul telecommunications. In the past, large efforts to push the InGaAs/GaAs system to this wavelength have been hampered by the large strain that accumulates in- and outside the QD structure during the Stranski-Krastanow growth leading to large increase of the local InAs band gap. Therefore, most recent developments aimed at the reduction of strain in the system that can be achieved by introducing metamorphic buffers[5] and thus replacing GaAs by InGaAs as matrix material close to the QD or by turning to InP as a completely different host material, which is employed our case. Both approaches reduce the lattice mismatch and limit the strain in the QD system.[6] The smaller lattice mismatch, however, carries the danger of creating too large QDs during the epitaxy, resulting in a small QD density and insufficient gain. This can be circumvented by using the (311)*B* substrate orientation,[7–9] resulting in high QD densities and low size dispersion, permitting the development of low-threshold QD lasers.[10] The height of our QDs (i.e., the wavelength emission) is well controlled using the "double-cap procedure."[6]

While the experimental impact of the substrate orientation on QD optical properties has been already studied by various groups,[11–14] still no complete theoretical study has been performed on these QDs grown on (N11) surfaces, matching the experimental datas.[15–21] Otherwise, a lot of theoretical work being in agreement with experimental data has been performed on other III-V system based QDs grown on (100) substrate orientation like InGaAs/GaAs or GaAs/AlGaAs, using either atomistic models, such as the empirical pseudopotential theory,[22–24] or continuum models, such as the eight-band $\mathbf{k}\cdot\mathbf{p}$ theory.[25–30]

In this paper, we theoretically investigate the impact of substrate orientation on the QDs optical properties, using the eight-band $\mathbf{k}\cdot\mathbf{p}$ model including strain and piezoelectric effects, and demonstrate that the use of the (311)*B* substrate breaks the initial symmetry of the (100) system, thus modifying the optical properties of the QDs.

From atomic force microscopy (AFM) measurements and cross-sectional scanning tunneling microscopy (X-STM), it is shown that a truncated cone shape can be assumed for capped QDs. Furthermore, as the "double cap" (DC) technique is used in our group to control the QD height and so the wavelength emission,[6] the QD height is used as an adjustable parameter both in experiment and simulation. Calculations based on the eight-band $\mathbf{k}\cdot\mathbf{p}$ model, including strain and piezoelectricity, and the configuration interaction model are thus performed for several QD heights.[29] The electronic and optical properties are thus deduced for InAs/InP QDs on (311)*B* and (100) substrate orientations. A comparison with experimental results confirms the accuracy of the model. The impact of substrate orientation on optical and electronic properties (ground and excited states transitions) is thus demonstrated. It is then interpreted in terms of different strain contributions to the transition energy for both substrates. The whole calculated optical spectra are then compared for (100) and (311)*B* substrate orientations, and the impact of the system symmetry (crystal and QD shapes) on the anisotropy of the wave function in such a substrate (311)*B* is discussed.

II. QD GEOMETRY

Recent growth developments have allowed us to reach high-quality InAs/InP QDs.[7–9] As these QDs are flat, their

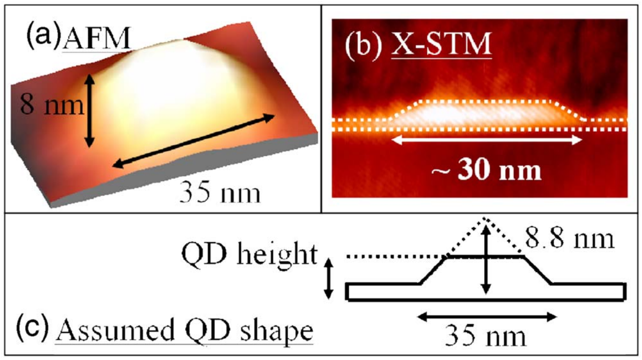

FIG. 1. (Color online) Structural investigations on InAs/InP QDs on (311)B-oriented substrate. From (a) atomic force microscopy (AFM), where the bright areas represent the top of the QD, and from (b) cross-sectional scanning tunneling microscopy (X-STM), where the bright areas represents the rich InAs area, a typical truncated cone-shaped QD geometry (c) can be assumed for calculations, where the QD height is a tunable parameter.

emission wavelength (on the ground state transition) is mainly related to their height, and can thus be controlled by the "double-cap" (DC) procedure.[6] From this procedural point of view, it becomes very important to understand the influence of the QD height on optical transitions. However, the electronic structure of QDs states depends also on the QD shape and lateral extension. In this regard, detailed structural investigations are necessary to describe, in a realistic way, the QD electronic structure. Figure 1(a) represents an atomic force microscopy (AFM) picture of a typical InAs/InP dot on (311)B substrate. The average height for this kind of dot with an average cylindrical symmetry is about 8 nm, while the diameter is about 35 nm. From this figure, it appears that the QD base resembles more a circle rather than a square. This property is likely to be maintained during the capping procedure. Therefore, we used a model QD having a circular base rather than one with a square base. But from AFM pictures, no precise idea about the three-dimensional (3D) shape of the QD can be obtained, as we have to take into account the tip effect, and most important the fact that in this measurement, the QDs are uncapped. Thus, X-STM measurements have also been performed in an ultrahigh vacuum (UHV) chamber with base pressure $<4.10^{-11}$ Torr on the UHV-cleaved $(01\bar{1})$ cross-sectional surface. Tips were prepared by electrochemical etching of polycrystalline tungsten wires and treated in the vacuum with a self-sputtering technique.[31–33] In Fig. 1(b), we show the X-STM picture of one InAs QD grown on InP (311)B substrate. In this picture, the QD, deposited on an InP surface, is simply capped with quaternary alloy $In_{0.8}Ga_{0.2}As_{0.435}P_{0.565}$, in order to avoid any intermixing effects (due to As/P exchanges). This figure (in a two-dimensional [2D] view) reveals a truncated, faceted profile of the QD. This figure also shows that the wetting layer (WL) has to be taken into account in the calculations, as its height is not small compared to the one of the QD. These two structural considerations (combination of the 2D and 3D views) allow us to propose a typical geometry for QDs in the calculations, given in Fig. 1(c). In the calculations, we assume the QDs to have a truncated faceted profile (from the 2D X-STM view) with a circular basis (from the 3D AFM view), where the total height of the QD is equal to 8.8 nm [30 monolayers (ML), where 1 ML ~ 0.29 nm on (100) substrate], and the base length is equal to 35 nm. We also do not consider any intermixing effects (As/P exchanges) that could occur on capped InAs/InP QDs. However, as we don't have any X-STM structural measurement of the in-plane structure of the QD, we assume a cylindrical symmetry (like the one observed by AFM for the uncapped QD), although it is well known that some anisotropy may be present on (311)B substrate and even more on (100) substrate.[34] This choice has been motivated by the sole comparison of the (100) and (311)B substrate effects. Indeed, if we take the [100] direction as a reference, the chosen QD geometry has the highest possible symmetry $C_{\infty v}$ on (100) substrate. This symmetry is reduced to C_{4v} when a continuum model is used, without interfacial symmetry, atomistic strain nor piezoelectricity.[24] No splitting of excited P states is predicted. When the atomistic symmetry is taken into account (piezoelectricity in our case), the symmetry is one more time reduced to C_{2v} if we take into account the zinc-blende crystal symmetry.[24] In this case, a weak splitting of excited p states is expected. Note that the values given in Ref. 24 are proposed for InAs/GaAs QDs, where the lattice mismatch is larger, so that the splitting in InAs/InP QDs should be even weaker. On (311)B substrate orientation, the initial symmetry of the considered QD is also $C_{\infty v}$. When the atomistic symmetry is taken into account, this symmetry is drastically reduced to $C_s=(E,\sigma)$, where σ is the $(01\bar{1})$ plane symmetry. In this case, no degeneracy of the excited states is expected, whatever the QD shape is. The structure loses every rotational C_v symmetry, as the initial $C_{\infty v}$ symmetry of the QD structure is not compatible at all with the crystal symmetry. This symmetry loss is expected to have drastic consequences on electronic and optical properties of QDs on (311)B substrate. In this context, calculations are performed for truncated cone-shaped InAs/InP QDs of various heights [8 ML (1ML ~ 0.29 nm), 10 ML, 12 ML 16ML and 30 ML], and for two different wetting layer heights (2 ML and 4 ML).

III. InAs/InP QDs ABSORPTION SPECTRA

A. About the InAs/InP confinement potential

Deeper insight into the electronic properties can be gained by comparing the InAs/InP QDs considered here to the archetypal InAs/GaAs system. In Fig. 2, the confinement potential of the two systems are compared for a truncated pyramid grown on (100) substrate. In the central section [Fig. 2(b)], the positions of the unstrained band edges relative to InAs are shown. Although the band-gap ratio of QDs and matrix material is very similar in both systems, the band offsets are different, reflecting the fact that InAs/GaAs share a common anion whereas InAs/InP share a common cation. In the presence of strain, the band-edge energies are altered [see Fig. 2(a) for InAs/InP and Fig. 2(c) for InAs/GaAs] by hydrostatic strain, mainly affecting the conduction band and by biaxial strain, thus lifting the heavy (light) hole degeneracy at the Γ point. The quantitative effect is much bigger

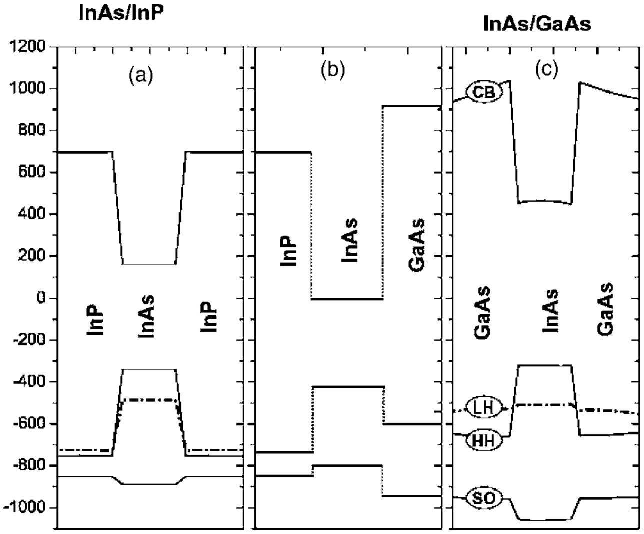

FIG. 2. Vertical scan through the confinement potential for an InAs QD embedded in InP (a) and GaAs (c). In the center (b), the energetic positions of the unstrained band edges for InP and GaAs relative to InAs are given.

for InAs embedded in GaAs due to the larger lattice mismatch (6.6% compared to only 3.1% for InP) and the accompanying increase of hydrostatic strain.

The most striking feature is the much smaller (strained) band gap of InAs in InP than in GaAs, which opens the door to reach the 1.55 μm emission for confined carriers, which is hard to achieve for InAs/GaAs QDs. Since the depth of the electron confinement potential is similar in both systems, one can expect a comparable spectrum for confined electron states, provided the QDs share the same morphological properties. This does not hold for hole states, since the confinement potential for InAs/InP QDs is much deeper and the heavy (light) hole splitting is smaller.

The material parameters entering the $\mathbf{k}\cdot\mathbf{p}$ analysis are taken from Ref. 27 for InAs and from Ref. 35 for InP.

B. Predicted absorption spectra of truncated cone-shaped InAs/InP QDs

Excitonic properties are now calculated for self-organized QDs based on a three-dimensional implementation of the eight-band $\mathbf{k}\cdot\mathbf{p}$ model and a configuration interaction scheme thus accounting for the inhomogeneous strain distribution, the piezoelectric effect, inter- and intraband mixing, and Coulomb interactions.[27,30] The modeling process starts with an assumption on shape, size, and composition, guided by structural investigations (see Sec. II on AFM and X-STM measurements). Next, the strain distribution and the piezoelectric potential are calculated, using the strain-dependent eight-band $\mathbf{k}\cdot\mathbf{p}$ Hamiltonian.

The strain distribution is calculated here using the continuum mechanical model, presented by Stier *et al.*,[27] which has demonstrated that this model is adapted to describe QD nanostructures with good accuracy.[27] In this model, the total strain energy is given by

$$U_{CM} = \frac{1}{2}\sum_{i,j,k,l} C_{ijkl}\varepsilon_{ij}\varepsilon_{kl}.$$

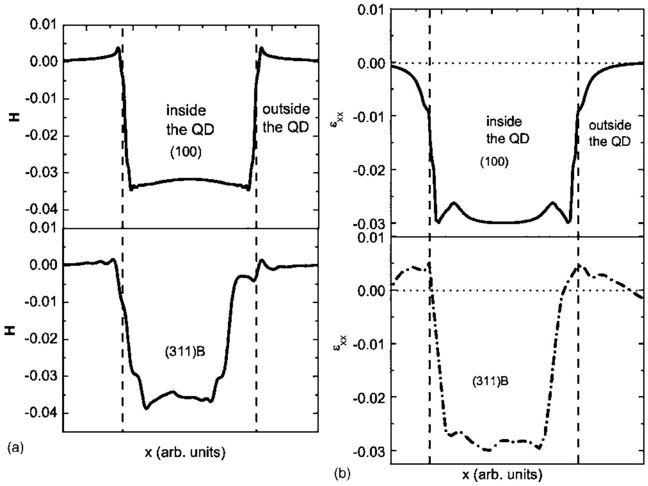

FIG. 3. (a) Hydrostatic strain components $H=\varepsilon_{XX}+\varepsilon_{YY}+\varepsilon_{ZZ}$ for (100) and (311)B substrates represented in the direction [010] for a truncated cone QD with 3.5 nm height. The spatial variation (b) of the deformation ε_{XX} cannot be compared directly because of the representation basis choice. However, the different hydrostatic strain values in the center of the QD for (100) and (311)B substrates should have a consequence on energy levels.

For a given structure, this energy is minimized, using finite differences for the strains $\varepsilon_{ij}=\partial u_i/\partial x_j$, where u is the displacement vector field. The compliances C_{ijkl} are represented by the parameters C_{11}, C_{12}, and C_{44} for cubic crystals. Other details of the calculations are presented in Ref. 27. The hydrostatic strain component $H=\varepsilon_{XX}+\varepsilon_{YY}+\varepsilon_{ZZ}$ is presented in Fig. 3(a) for (100) and (311)B substrates, along the direction [010] for a QD with a height of 3.5 nm. Even if the spatial variation of the hydrostatic strain cannot be compared directly between (100) and (311)B substrates, values of the hydrostatic strain in the center of the QD are −0.032 and −0.036 respectively for (100) and (311)B substrates. This implies that hydrostatic strain contributions to the energy levels should be different for (100) and (311)B substrates. Figure 3(b) shows the ε_{XX} component of the deformation tensor, along the [010] direction. While the values of this component in the center of the QD are the same for both substrates orientations, it is clearly visible that a direct comparison of both strain components cannot be performed directly, as the (311)B structure is rotated in the calculation box. Indeed, the deformation tensor represented here in the $X=[010]$ and $Y=[001]$ basis should be represented into the $X'=[01\bar{1}]$ and $Y'=[\bar{2}33]$ in the case of the (311)B substrate. As a consequence, positive values of ε_{XX} are calculated at the edge of the QD for the (311)B substrate orientation (apparition of shear components) on Fig. 3(b). Strain calculation themselves not being the center of this article, the strain contributions to the single-particle energies will be analyzed, as they can be compared directly without any rotation of the system.

By solving the Schrödinger equation, we obtain single-particle wave functions. The parameters entering this Hamiltonian are based on experimental values for the required bulk material Γ-point band structure parameters.[35] Free adjustable parameters are not present in this model. Figure 4 displays

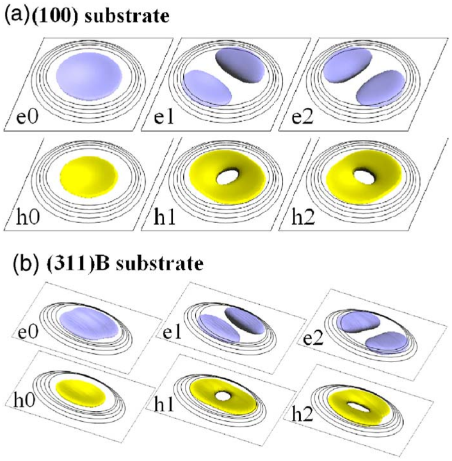

FIG. 4. (Color online) Wave function representations for electrons and holes for the first QDs states on (100) substrate orientation (a) and on (311)*B* substrate orientation (b), with a QD height of 2.93 nm. *e*0, *e*1, and *e*2 stands for electronic states 1*Se* and 1*Pe*. *h*0, *h*1, and *h*2 stands for hole states 1*Sh* and 1*Ph*. The (311)*B* substrate induces an anisotropy of the wave function.

the first three electron and hole wave functions (70% isosurface) for both the (100) and the (311)*B* substrate, as a result of step (c), for illustration. The symbols *e*0 and *h*0 stands for 1*Se* and 1*Sh* states (i.e., with an in-plane "*S*-like" symmetry for electrons and holes). *e*1, *e*2, *h*1, *h*2 stands for 1*Pe* and 1*Ph* states (i.e., with an in-plane "*P*-like" symmetry for electrons and holes). The terms "*S*-like" and "*P*-like" are used here, in order to make the parallel with the usual notation of states in the cylindrical symmetry.[21] The single-particle states provide a basis for the configuration interaction model, which is applied to calculate excitonic properties, including correlation and exchange.[30] Finally, the excitonic optical absorption spectra are computed.

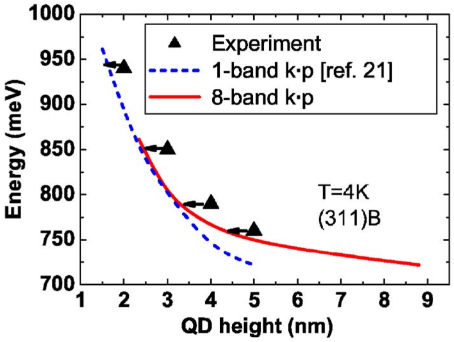

FIG. 5. (Color online) predicted (solid line for eight-band **k·p**, dashed line for one-band **k·p** [Ref. 21]) and observed (solid symbols) energies of the ground exciton transition in truncated cone-shaped InAs/InP (311)*B* QDs as a function of QD height. The eight-band **k·p** predicted transitions have a better agreement with the experimental data than the one-band **k·p** predicted transitions.

By using this procedure, good agreement between experiment and prediction still needs to be demonstrated. In order to check the validity of the used model, the eight-band **k·p** ground transitions are to be compared to those determined by photoluminescence experiments performed on InAs/InP (311)*B* QDs. Figure 5 represents the 1*Se*-1*Sh* ground transition energies measured (triangles), calculated by one-band **k·p** approximation in Ref. 21 (dashed line), and calculated by height-band **k·p** method in this work (straight line) as a function of QD height. The photoluminescence experiments were carried out at 4.2 K in a He bath cryostat. The photoluminescence is excited using a cw Krypton laser (647 nm wavelength) at 1 mW, in order to avoid any state filling at high energy. The samples are designed to have different first capping layer heights, thus having different InAs/InP QDs heights (2 nm, 3 nm, 4 nm, 5 nm), using the double-cap procedure.[6] Hence, the comparison between experiment and calculations can be performed using ground state transition energy as criterion. While the experimental energies are determined with high accuracy, the height of our QDs reported on the horizontal scale of Fig. 5 is an approximation of the real QD height. Indeed, in first approximation, the experimental QD height proposed in Fig. 5 is set equal to the deposited height of InP in the first step of the double-cap procedure. However, from the analysis of the growth mechanisms when the DC procedure is used, it is commonly accepted that the deposited height of InP during the first cap is a little bit larger (2 ML) than the effective height of the QD.[6] So, the eight-band **k·p** calculations are in good agreement with experimental data, provided a simple translation of QD height along the horizontal scale can be performed (shown by arrows in Fig. 5). Figure 5 also shows the limitation of a simple model such as the one-band approximation, especially for higher QDs,[21] and justifies the use of the eight-band **k·p** model.

Figure 6 displays calculated exciton absorption spectra for QDs of different height on (100) substrate, as an illustration of the output of the calculations (the WL height in this case is taken equal to 4 ML). Calculated exciton absorption spectra are plotted with a polarization along the $[01\bar{1}]$ axis, as this axis is a QD in-plane axis for both substrates. In this case, the exciton binding energy is on the average equal to 15.5 meV. The spectra show a blueshift of 135 meV for the ground state transition energy upon reducing the QD height from a pointed cone-shaped QD down to an 8 ML truncated

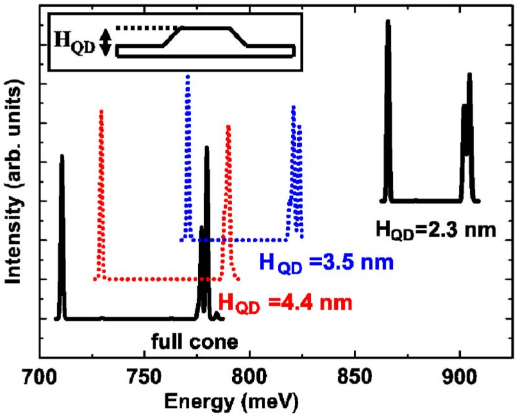

FIG. 6. (Color online) Excitonic absorption spectra calculated in an eight-band **k·p** model for InAs/InP (100) QDs, as a function of the QD height for a polarization along the $[01\bar{1}]$ direction. A truncated cone-shaped QD with a base length of 35 nm was assumed.

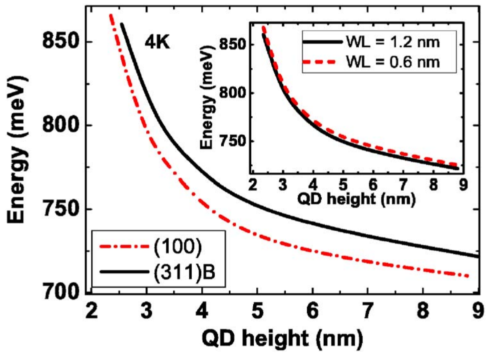

FIG. 7. (Color online) Comparison between calculated ground state exciton transition energy in InAs/InP (311)B QDs (solid line) and InAs/InP (100) QDs (dotted line), as a function of QD height. The difference between both curves is mainly related to hydrostatic strain. The inset shows the weak influence of the WL dimension (1.2 nm, solid line; 0.6 nm, dashed line) on ground state exciton transitions in InAs/InP (311)B QDs.

one. It is also seen on Fig. 6 that excited states are energetically closer for flat quantum dots compared to the full cone. This is explained by the different aspect ratio of considered QDs. Indeed, in the case of flat QDs, the weak lateral confinement has only few consequences on Px and Py states energy shift, while the strong vertical confinement has a large impact on the ground S state energy increasing. Ground and excited transitions are thus energetically closer for flat QDs than for the full-cone QD. The spectrum calculated with height-band $\mathbf{k}\cdot\mathbf{p}$ calculations on Fig. 6 provides much more richness compared to those found with previous calculations.[21] In this regard, a comparison between (311)B QDs and (100) QDs absorption spectra is to be made.

IV. IMPACT OF SUBSTRATE ORIENTATION ON QD OPTICAL PROPERTIES

A. Ground state transition on (100) and (311)*B* substrates

In Fig. 7, the exciton ground state (X_0) transition energy is plotted as a function of QD height for the two different substrate orientations (100) and (311)B, whereof we can derive two main results: (1) The smaller the QD height is, the larger becomes the X_0 transition energy, also known as the quantum-size effect. (2) Whatever the QD height is, the X_0 transition energy is always larger for (311)B grown QDs than for the (100) grown QDs. To understand this last point, we have to analyze (a) the electron and hole ground state energies and (b) the X_0 binding energy.

(a) The single particle energies: The electron ground state energy can be separated into the components $E=E_{\text{quant}}+E^{0}_{\text{conf}}+E^{\text{strain}}_{\text{hydro}}+E_{\text{piezo}}+E_{\Delta}$, where E_{quant} represents the kinetic part of the Hamiltonian, $E_{\text{hydro}}=\langle\Psi|a_c(\varepsilon_{xx}+\varepsilon_{yy}+\varepsilon_{zz})|\Psi\rangle$ is the energy shift induced by hydrostatic strain with a_c being the conduction band deformation potential, $E_{\text{piezo}}=\langle\Psi|V_{\text{piezo}}|\Psi\rangle$ is the energy shift induced by the internal piezoelectric field, and $E^{0}_{\text{conf}}=\langle\Psi|V_{\text{conf}}|\Psi\rangle$ is the confinement energy related to the unstrained position of the local conduction band. This energy becomes minimal if the wave function is completely localized inside the QD and increases the more it spreads into the barrier material. Hence, it is a measure for the "spreading out" of the wave function in question. E_{Δ}, not being quantified here, contains the energy contributions induced by the nondiagonal components of the Hamiltonian related to the strain tensor (tetragonal and shear deformation) and coupling to the valence band. For hole states, an additional term $E^{\text{strain}}_{\text{biaxial}}=\langle\Psi|b(\varepsilon_{xx}+\varepsilon_{yy}-2\varepsilon_{zz})|\Psi\rangle$ appears reflecting the influence of the biaxial strain with b being the shear deformation potential. The fact that for all investigated QDs the transition energy is higher if the dots are placed on (311)B substrate than on (100) substrate is not surprising since the hydrostatic strain energy shift is larger for (311)B grown QDs, $[E_{\text{hydro}}(e_0)](311)>[E_{\text{hydro}}(e_0)](100)$, as it has already been demonstrated in Miska *et al.*[21] The difference of this contribution in our calculations is found to be 10 meV for tall (30 ML) and 15 meV for flat (8 ML) QDs [see Fig. 8(c)]. Resulting from the larger strain inside the (311)B QDs, the conduction band offset becomes smaller and the wave function "spread out" becomes larger. Therefore, the confinement energy related to the unstrained local conduction band $E^{0}_{\text{conf}}(e_0)$ increases and the quantization energy $E_{\text{quant}}(e_0)$ decreases for (311)B QDs compared to their (100) grown counterparts, as can be seen in Figs. 8(a) and 8(b). For the (311)B, there are some minor contributions from the piezo-

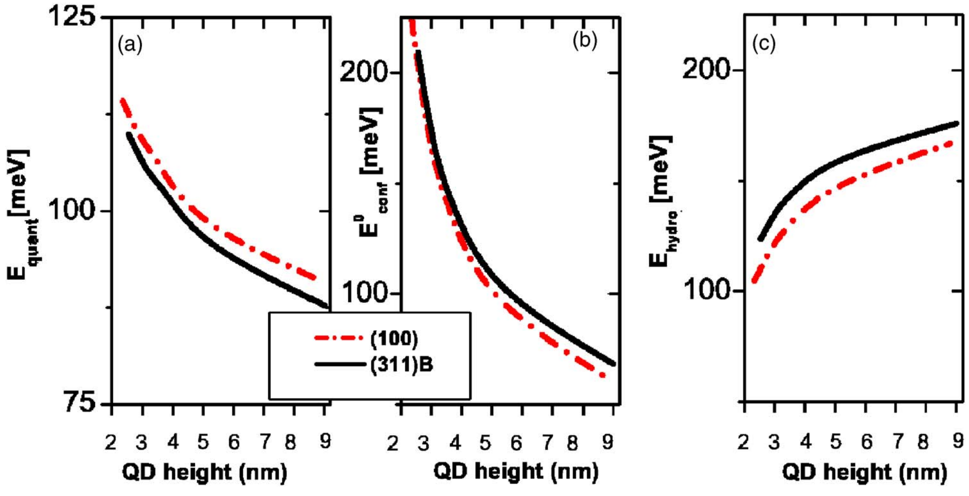

FIG. 8. (Color online) The electron ground state energy for different QD heights decomposed into the quantization energy E_{quant}(a), confinement energy $E^{0}_{\text{conf}}(b)$, and the energy shift induced by hydrostatic strain $E^{\text{strain}}_{\text{hydro}}(c)$ the two substrate orientations (100) and (311)B. E_{piezo} is not shown since it is close to zero for the electron ground state.

electric potential even for the electron ground states, which are not present in the (100) case. We find an energy drop of 3.2 meV for the tallest and 0.4 meV for the flattest (311)B QD. This is due to the fact that in this case the piezoelectric potential [see Fig. 10(b)] breaks any symmetry that might be present from the QD shape, thus pulling the electron states to one QD side and the hole states to the other. In the (100) system, the carriers are instead getting distorted but their (x,y) component of the wave function barycenter still coincides with that of the QD structure.

(b) The X_0-binding energy: The X_0 binding energy is foremost a function of the extent of the electron and hole wave function and their mutual positions. Therefore, since the electron ground states of the (311)B QDs exhibit a "spread out," visible in the smaller quantization energy $E_{\text{quant}}(e_0)$, and as the barycenter of Ψ_{e0} and Ψ_{h0} are slightly drawn apart by the particular piezoelectric field, we find a smaller X_0 binding energy for these (311)B QDs. The difference $\Delta E_{X0} = E_{X0}(100) - E_{X0}(311)$ to the (100) QDs, however, is very small—in the order of 2 meV, which is not enough to compensate the blueshift caused by the larger hydrostatic strain of the (311)B QD system.

The exciton energy difference between both substrates given in Ref. 21 is, however, larger than those calculated in this work. In this reference, however, the influence of E_{piezo} and possible variations of E_{quant} (due to effective mass variations) have not been taken into account.

In this regard, the part of the Hamiltonian related to the strain tensor, including hydrostatic and shear deformations, plays the main role in explaining the difference between (311)B and (100) substrates for small QDs. As the difference between shear/tetragonal and hydrostatic deformations on (100) and (311)B has already been demonstrated,[36] and as the impact of these deformations on electronic properties has been already observed,[15] we propose to interpret the difference between (311)B and (100) for several QDs heights as a direct consequence of shear/tetragonal and hydrostatic deformations difference on these substrates. As an illustration, the energy shift induced by the piezoelectric field on (311)B has also been demonstrated experimentally on (311)B QDs.[13] In summary, the difference observed for large QDs on (311)B and (100) substrate is mainly due to the hydrostatic strain.

The influence of the WL thickness on QD ground state is also studied in the Fig. 7 inset. In our previous work, we showed that the WL is expected to play a role in the electronic structure of QDs.[8] The QD ground state transition is plotted for two different structures with a WL thickness of respectively 0.6 (2 ML) and 1.2 nm (4 ML). As expected, the QD ground state transition energy for the largest WL thickness is smaller than for the smallest WL thickness. This is explained by the difference between ground state wave function penetration in the WL.[8] The next results presented in this paper come from calculations made on structures with a WL thickness of 1.2 nm. This choice is motivated by the measured WL thickness by X-STM, which is around 1 nm.

B. QDs absorption spectra on (100) and (311)B substrates

The complete analysis for the whole absorption spectrum can be performed on (100) and (311)B substrates. Figure 9 represents the comparison of full-cone (30 ML) absorption spectra for QDs grown on the two different substrates. Figures 10(a) and 10(b) represent excitonic transition energies for both substrate orientations as a function of QD height. These transitions are derived from absorption spectra polarized along the $[01\bar{1}]$ direction (as the one in Fig. 9), that is, an in QD plane direction for both substrates. Despite the different substrate orientations, the energy and the splitting of the P-like state transitions foremost depend on the QD size and hardly on the orientation of the substrate. The splitting of these transitions, ΔE_P is related to the presence of the piezoelectric field,[27] which lifts the degeneracy of the electron and hole p states even in the presence of the structural $C_{\infty v}$ symmetry. Despite the fact that the magnitude of ΔE_P is very similar for both substrate orientations, the piezoelectric field itself is very different in its strength and symmetry, as

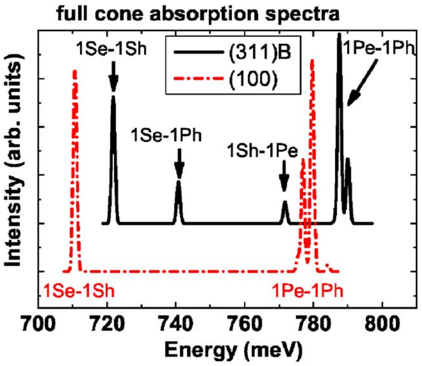

FIG. 9. (Color online) Comparison between full-cone (30 ML) QDs absorption spectra for the two substrates orientations (311)B and (100).

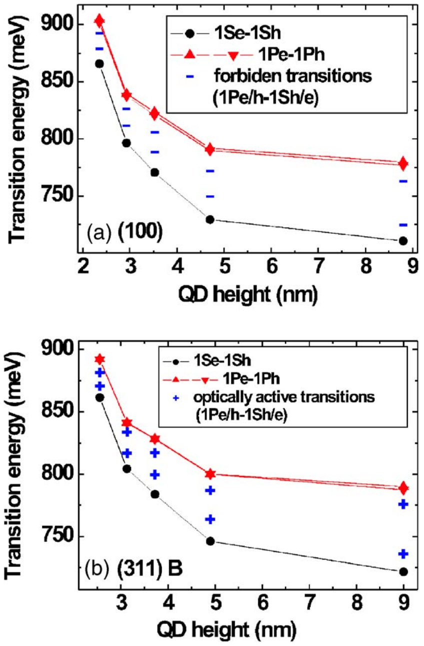

FIG. 10. (Color online) Comparison between calculated transitions in InAs/InP (100) QDs (a) and InAs/InP (311)B QDs (b), as a function of QD height. On (311)B substrate, second-order transitions (+) become optically active.

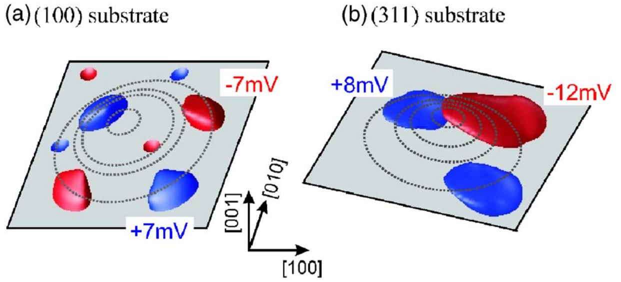

FIG. 11. (Color online) Orientation and appearance of the piezoelectric potential (isosurface plot) for QDs grown on (100) and on (311)*B* substrates.

can be seen in Fig. 11: for the (100) QD, the lobes of the positive and negative isosurface are congruent and can be transformed into each other just by a rotation of $\pi/2$, which is in striking contrast to the (311)*B* QD. This one exhibits no apparent symmetry and, moreover, the maxima of the positive and the negative part of the potential are not even equal: for the QD shown in Fig. 11(b), the piezoelectric potential ranges from $\min(V_{\text{piezo}})=-25.2$ mV to $\max(V_{\text{piezo}})=12.8$ mV, in contrast to ±8.5 mV for the (100) QD in Fig. 11(a).

In both cases the *p*-channel splitting is also a function of QD size, and is related to the size dependence of the piezoelectric field in QDs. The latter effect is well known for (100) QDs for a longer time,[27] and holds also for (311)*B* QD as can be seen from the values listed in Table I. The much larger magnitude of the piezoelectric field in (311)*B* QDs, however, is not reflected in the *p*-channel splitting, since the former is not symmetry adapted to the *p* states as it is tilted against the substrate orientation.

Another difference between the two substrates that is linked to the orientation of the piezoelectric field appears in Fig. 9. While on the (100) substrate [Fig. 10(a)] the absorption spectra are mainly constituted of first-order transitions (1*Se*-1*Sh*, 1*Pe*-1*Ph*), the (311)*B* absorption spectra [Fig. 10(b)] also reveal second order-transitions (1*Se*-1*Ph*, 1*Pe*-1*Sh*), as is illustrated in Fig. 9 for the QD with a 30 ML height (full cone). The (311)*B* substrate is thus expected to activate these second-order transitions, which are usually considered as "forbidden" transitions without excitonic effects in $C_{\infty v}$. For QDs having at least C_{2v} symmetry, the integral between the envelope functions of the electron *p*-state Ψ_{e1} and the hole *s*-state $\Psi_{h0}\langle\Psi_{e1}|\Psi_{h0}\rangle$ (almost) disappear since the envelopes belong to different irreducible representations of the symmetry group. The term "almost" is related to the fact that even the hole ground state carries some light hole character, which can add new symmetry properties to the envelope rendering the whole wave function a reducible representation. For the (311)*B* QD the barycenter of the hole ground state is pulled to one QD side and that of the electron *p* state to the other side. Therefore, the integral $\langle\Psi_{e1}|\Psi_{h0}\rangle$ cannot vanish anymore for symmetry reasons and the transitions (1*Se*-1*Ph*, 1*Pe*-1*Sh*) are not forbidden anymore and become activated. However, the smaller the QDs and hence the piezoelectric field become, the weaker these transitions are.

TABLE I. The strength of the piezoelectric potential as a function of QD size and substrate orientation.

QD height (nm)	Substrate orientation	Min (V_{piezo}) (mV)	Max (V_{piezo}) (mV)
2.3	(100)	−2.5	2.5
2.5	(311)*B*	−10.6	7.9
8.8	(100)	−8.5	8.5
9.0	(311)*B*	−25.2	12.8

In conclusion, all the observed differences between the two substrates can be linked to the lack of symmetry on the (311)*B* substrate, which results in larger shear strain becoming manifests through the piezoelectric field.

C. Discussion

Indeed, the optically activated "forbidden" transitions for the (311)*B* QDs raise the problem of symmetry in this system. The problem of the impact of symmetry on calculations and predicted optical properties in QDs have been already studied by Bester and Zunger.[24] However, in this reference, QDs are considered only on the (100) substrate orientation. In our case, we have shown that taking into account the crystal symmetry leads to consider a C_{2v} symmetry for a QD grown on (100) substrate while the (311)*B* substrate induces a reduction of the symmetry down to $C_s=(E,\sigma)$. The main consequence of this loss of symmetry is the presence of a high value for shear strain and tetragonal deformation.[36] The wave function is then more sensible to the crystal orientation on (311)*B* than on (100) substrate, and especially for small QDs where the shear and tetragonal deformations play a very important role (the strain relaxation is less efficient). In this case, the wave function becomes clearly anisotropic, and depends a lot of crystal orientation [whatever the QD shape is in this (311) system]. This loss of symmetry thus have drastic consequences on wave-function symmetries. In the C_{2v} symmetry considered for the (100) substrate, eigenstates calculated from the eight-band $\mathbf{k}\cdot\mathbf{p}$ Hamiltonian have nearly the 1*S* and 1*P* symmetries. A very weak splitting of *p* states is observed, as the C_{4v} to C_{2v} reduction of symmetry is small, and only has a few consequences on the calculation of energy levels. In this case, *p*-states are respectively elongated along the [011] and $[01\bar{1}]$ directions. In the C_s symmetry considered for the (311)*B* substrate, eigenstates do not have such a symmetry any more. Thus, the ground state is not a pure *s* state, and excited states are not pure *p* states. Excited states are then aligned along $[01\bar{1}]$ and $[\bar{2}33]$ directions, with a strong difference between both directions. The difference between the two directions is large, as we are far from the C_{4v} symmetry, unlike to the (100) substrate. Then, if the eigenstates found in our system cannot be written diagonally on the $\{S;P\}$ representation, nonzero cross terms appear in this representation. The optical activation of cross transitions is one of the main consequences. The complete analysis has been already done by Stier *et al.*[27] This phenomenon is greatly enhanced on the $(311)B$ substrate. Thus, the wave function in such a low-symmetrical configuration becomes much more sensible to the crystal symmetry, and less sensible to QD symmetry. In this paper, we have considered a truncated conical-shaped QD; however, the conclusion presented here can be extended to all possible shapes assumed for QDs on $(311)B$ substrates. Moreover, in this paper, the main emphasis has been given to the understanding of the different contributions to the electronic levels in the conduction band. However, the same development could be performed on valence band eigenstates. In this analysis, the impact of the loss of symmetry on $(311)B$ substrate becomes harder to determine, as the calculations performed take into account the band mixing effects *LH-HH* in the valence band. This study of valence band would also lead to describe the sensitivity to the polarization of optical transitions. In this polarization study, the loss of symmetry should induce a large difference between QDs grown on $(311)B$ and (100) substrates. Further theoretical investigations will be done in order to understand this polarization dependence of optical transitions on both $(311)B$ and (100) substrates.

V. CONCLUSION

The impact of substrate orientation on the electronic and optical properties of QDs has been studied theoretically in this work. Based on AFM and X-STM measurements, it has been demonstrated that eight-band $\mathbf{k}\cdot\mathbf{p}$ calculations performed on truncated conical-shaped QDs show a good agreement with photoluminescence measurements performed on $(311)B$ substrate, for various QDs heights. Next, we found that QDs grown on $(311)B$ and (100) substrate exhibit different excitonic optical signatures mainly for two reasons: First, the larger hydrostatic strain observed for the $(311)B$ QDs elevates the electron energies, thus causing an overall increase of the excitonic transition energy. Second, the way the piezoelectric field acts on both substrates is fundamentally different in view of its strength and its orientation. This alters the symmetry properties of the confinement potential and induces the optical activation of second-order transitions on the $(311)B$ substrate. Therefore, for this substrate orientation, the electronic and optical properties are considered to be less sensible to the QD geometry, and more sensible to the crystal orientation, than on (100) substrate orientation.

ACKNOWLEDGMENTS

This work was supported by the SANDiE Network of Excellence (Contract no. NMP4-CT-2004-500101) of the 6th Framework Programme of the European Commission and Sfb 296 of Deutsche Forschungsgemeinschaft. The calculations were carried out on the a IBM P690 supercomputer at HLRN within Project No. BEP00014.

---

*Corresponding author. Email address: charles.cornet@ens.insa-rennes.fr

[1] D. Bimberg, M. Grundmann, and N. N. Ledentsov, *Quantum Dot Heterostructures* (Chichester, Wiley, 1998).

[2] D. Bimberg, J. Phys. D **38**, 2055 (2005).

[3] M. Sugawara, *Self-Assembled InGaAs/GaAs Quantum Dots, Semiconductors and Semimetals*, Vol. 60 (Toronto, Academic, 1999).

[4] Zh. I. Alferov, *Quantum Wires and Dots show the Way Forward* (III-Vs Rev.), Vol. 11 (1998), p. 47.

[5] L. Ya. Karachinsky, T. Kettler, N. Yu. Gordeev, I. I. Novikov, M. V. Maximov, Yu. M. Shernyakov, N. V. Kryzhanoskaya, A. E. Zhukov, E. S. Semenova, A. P. Vasilev, V. M. Ustinov, N. N. Ledentsov, A. R. Kovsh, V. A. Shchukin, S. S. Mikhrin, A. Lochmann, O. Schulz, L. Reissmann, and D. Bimberg, Electron. Lett. **41**, 478 (2005).

[6] C. Paranthoen, N. Bertru, O. Dehaese, A. Le Corre, S. Loualiche, B. Lambert, and G. Patriarche, Appl. Phys. Lett. **78**, 1751 (2001).

[7] P. Caroff, N. Bertru, A. Le Corre, T. Rohel, I. Alghoraibi, H. Folliot, and S. Loualiche, Jpn. J. Appl. Phys., Part 1 **44**, L1069 (2005).

[8] C. Cornet, C. Platz, P. Caroff, J. Even, C. Labbé, H. Folliot, A. Le Corre, and S. Loualiche, Phys. Rev. B **72**, 035342 (2005).

[9] H. Saito, K. Nishi, and S. Sugou, Appl. Phys. Lett. **78**, 267 (2001).

[10] P. Caroff, C. Paranthoen, C. Platz, O. Dehaese, H. Folliot, N. Bertru, C. Labbé, R. Piron, E. Homeyer, A. Le Corre, and S. Loualiche, Appl. Phys. Lett. **87**, 243107 (2005).

[11] Zh. M. Wang, Y. I. Mazur, Sh. Seydmohamadi, G. J. Salamo, and H. Kissel, Appl. Phys. Lett. **87**, 213105 (2005).

[12] S. Sanguinetti, M. Gurioli, E. Grilli, M. Guzzi, and M. Henini, Appl. Phys. Lett. **77**, 1982 (2000).

[13] A. Patanè, A. Levin, A. Polimeni, F. Schindler, P. C. Main, L. Eaves, and M. Henini, Appl. Phys. Lett. **77**, 2979 (2000).

[14] Y. Temko, T. Suzuki, P. Kratzer, and K. Jacobi, Phys. Rev. B **68**, 165310 (2003).

[15] M. Povolotskyi, A. Di Carlo, P. Lugli, S. Birner, and P. Vogl, IEEE Trans. Nanotechnol. **3**, 124 (2004).

[16] J. B. Xia, Phys. Rev. B **43**, 9856 (1990).

[17] S. S. Li and J. B. Xia, Phys. Rev. B **50**, 8602 (1994).

[18] T. B. Bahder, Phys. Rev. B **51**, 10892 (1995).

[19] R. H. Henderson and E. Towe, J. Appl. Phys. **78**, 2447 (1995).

[20] P. Tomasini, K. Arai, F. Lu, Z. Q. Zhu, T. Sekiguchi, M. Suezawa, T. Yao, M. Y. Shen, T. Goto, T. Yasuda, and Y. Segawa, J. Appl. Phys. **83**, 4272 (1998).

[21] P. Miska, C. Paranthoen, J. Even, N. Bertru, A. Le Corre, and O. Dehaese, J. Phys.: Condens. Matter **14**, 12301 (2002).

[22] L. W. Wang, A. J. Williamson, A. Zunger, H. Jiang, and J. Singh, Appl. Phys. Lett. **76**, 339 (2000).

[23] L. W. Wang, J. Kim, and A. Zunger, Phys. Rev. B **59**, 5678 (1999).

[24] G. Bester and A. Zunger, Phys. Rev. B **71**, 045318 (2005).

[25] M. Grundmann, N. N. Ledentsov, O. Stier, D. Bimberg, V. M. Ustinov, P. S. Kop'ev, and Zh. I. Alferov, Appl. Phys. Lett. **68**, 979 (1996).

[26] F. Guffarth, R. Heitz, A. Schliwa, O. Stier, N. N. Ledentsov, A. R. Kovsh, V. M. Ustinov, and D. Bimberg, Phys. Rev. B **64**, 085305 (2001).

[27] O. Stier, M. Grundmann, and D. Bimberg, Phys. Rev. B **59**, 5688 (1999).

[28] A. Rastelli, S. Stufler, A. Schliwa, R. Songmuang, C. Manzano, G. Costantini, K. Kern, A. Zrenner, D. Bimberg, and O. G. Schmidt, Phys. Rev. Lett. **92**, 166104 (2004).

[29] R. Heitz, F. Guffarth, K. Pötschke, A. Schliwa, D. Bimberg, N. D. Zakharov, and P. Werner, Phys. Rev. B **71**, 045325 (2005).

[30] S. Rodt, A. Schliwa, K. Pötschke, F. Guffarth, and D. Bimberg, Phys. Rev. B **71**, 155325 (2005).

[31] P. Offermans, P. M. Koenraad, J. H. Wolter, K. Pierz, M. Roy, and P. A. Maksym, Physica E (Amsterdam) **26**, 236 (2005).

[32] Q. Gong, P. Offermans, R. Nötzel, P. M. Koenraad, and J. H. Wolter, Appl. Phys. Lett. **85**, 5697 (2004).

[33] P. Offermans, P. M. Koenraad, J. H. Wolter, K. Pierz, M. Roy, and P. A. Maksym, Phys. Rev. B **72**, 165332 (2005).

[34] S. Fréchengues, V. Drouot, N. Bertru, B. Lambert, S. Loualiche, and A. Le Corre, J. Cryst. Growth **201&202**, 1180 (1999).

[35] I. Vurgaftman, J. R. Meyer, and L. R. Ram-Mohan, J. Appl. Phys. **89**, 5815 (2001).

[36] L. De Caro and L. Tapfer, Phys. Rev. B **48**, 2298 (1993).